ACS APPLIED MATERIALS & INTERFACES

Research Article

www.acsami.org

Zirconium Tungstate/Epoxy Nanocomposites: Effect of Nanoparticle Morphology and Negative Thermal Expansivity

Hongchao Wu,[†] Mark Rogalski,[†] and Michael R. Kessler*[,†,‡,§]

[†]Department of Materials Science and Engineering, Iowa State University, Ames, Iowa 50011, United States

[‡]Ames Laboratory, U.S. Department of Energy, Ames, Iowa 50011, United States

[§]School of Mechanical and Materials Engineering, Washington State University, Pullman, Washington 99164, United States

ABSTRACT: The ability to tailor the coefficient of thermal expansion (CTE) of a polymer is essential for mitigating thermal residual stress and reducing microcracks caused by CTE mismatch of different components in electronic applications. This work studies the effect of morphology and thermal expansivity of zirconium tungstate nanoparticles on the rheological, thermo-mechanical, dynamic-mechanical, and dielectric properties of ZrW_2O_8/epoxy nanocomposites. Three types of ZrW_2O_8 nanoparticles were synthesized under different hydrothermal conditions and their distinct properties were characterized, including morphology, particle size, aspect ratio, surface area, and CTE. Nanoparticles with a smaller particle size and larger surface area led to a more significant reduction in gel-time and glass transition temperature of the epoxy nanocomposites, while a higher initial viscosity and significant shear thinning behavior was found in prepolymer suspensions containing ZrW_2O_8 with larger particle sizes and aspect ratios. The thermo- and dynamic-mechanical properties of epoxy-based nanocomposites improved with increasing loadings of the three types of ZrW_2O_8 nanoparticles. In addition, the introduced ZrW_2O_8 nanoparticles did not negatively affect the dielectric constant or the breakdown strength of the epoxy resin, suggesting potential applications of ZrW_2O_8/epoxy nanocomposites in the microelectronic insulation industry.

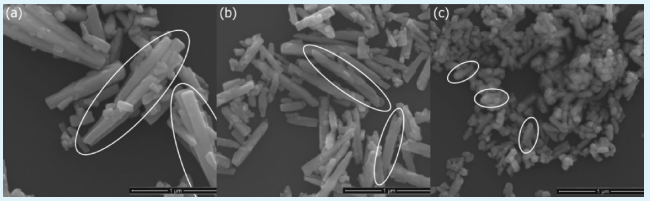

KEYWORDS: *negative thermal expansion, zirconium tungstate nanoparticle, polymer−matrix composites (PMCs), thermo-mechanical properties, dielectric properties*

1. INTRODUCTION

Epoxy resins belong to a subset of thermoset materials that find broad applications in the adhesives and construction materials industries. They exhibit excellent adhesion, advantageous heat and chemical resistance, superior mechanical properties, and good electrical insulating properties. In recent decades, epoxy resins were modified by adding various inorganic fillers to improve a variety of polymer properties, and numerous studies showed promising results. For example, layered silicate improved the dynamic modulus of epoxy resins;[1] the incorporation of carbon nanotubes enhanced the thermal and mechanical properties as well as the electrical conductivity of epoxy resins;[2,3] incorporation of ZnO nanoparticles into epoxy resin achieved high-UV shielding efficiency and high-visible light transparency;[4] and epoxy nanocomposites filled with silica nanoparticles achieved improved mechanical properties.[5] However, the high coefficient of thermal expansion (CTE) of epoxy resins limits their applications, especially in fields that demand extraordinary dimensional stability, such as high-performance structural materials in aerospace engineering or conformal coatings used in the microelectronics industry. The ideal candidates for these applications exhibit a tailored CTE in order to prevent premature failure, such as cracking, caused by thermal residual stresses generated at the interface by a CTE mismatch of two components. Therefore, various types of inorganic nanoscale reinforcements such as silica,[6−9] boron nitride nanosheets,[10] carbon nanotubes,[11,12] and clays[13] were studied to reduce the CTEs of different polymer materials. However, the extent of CTE reduction is constrained by the low but positive CTE values of these filler materials. It is assumed that employing a filler with a negative thermal expansion value can provide additional reductions in CTE of the polymer composite at lower loadings.

Zirconium tungstate (ZrW_2O_8), characterized by a cubic crystal structure and space group $P2_13$ in the α-phase, exhibits strong and isotropic negative thermal expansion (NTE) behavior over a wide temperature range (from 0.3 to 1050 K).[14] The NTE behavior in zirconium tungstate originates from the counter-rotations of WO_4 and ZrO_6 polyhedra in the crystal structure, initiated by the transverse thermal vibration of the shared oxygen atom connecting the polyhedra.[15] In recent years, ZrW_2O_8 has attracted growing research interest for its potential use as a filler in composite materials to control thermal expansivity and eliminate residual thermal stress. Although several reports revealed that ZrW_2O_8 can also be incorporated into metal and ceramic-based composites,[16−19] the majority of matrix materials used are polymeric, including epoxy resins,[20−22] polyimides,[23−25] phenolic resins,[26] and

Received: June 9, 2013
Accepted: September 16, 2013
Published: September 16, 2013

cyanate esters.[27−29] The CTEs of polyester/ZrW_2O_8 and epoxy/ZrW_2O_8 composites with 30 vol % of filler loading were reduced from 94 and 54 to 56 and 18 ppm/K, respectively.[30] Tani et al.[26] found that the CTE of phenolic resin composites decreased from 46×10^{-6} to 14×10^{-6} K^{-1} by incorporating up to 52 vol % of ZrW_2O_8 filler. Badrinarayanan et al.[27] observed that the CTE of bisphenol E cyanate ester (BECy) decreased by 92% in its glassy phase with 65 vol % filler loading. ZrW_2O_8 exhibited a catalytic effect on the cure behavior of BECy resin.[31] Badrinarayanan and Kessler[28] reported a 20% reduction in the CTE of BECy resin with 10 vol % nanosized ZrW_2O_8 incorporated to improve filler dispersion and ease of processing. Certain surface modifications of nanoparticles are also essential to improve the compatibility of oxide fillers with the matrix materials, depending on the type of polymer.[32] For example, when ZrW_2O_8 was surface-derivatized by 3-aminopropylsiloxy linker molecules, a 22 vol % loading in a polyimide resin led to a 30% reduction in CTE of the composite.[23] Recent work[22] also reported that epoxy resin reinforced by unfunctionalized nanoparticles with hydroxyl groups terminated on the surface exhibited better thermal-mechanical properties than epoxy containing silane-functionalized nano-ZrW_2O_8 and amine functional groups.

However, the effect of the ZrW_2O_8 nanoparticle morphology on the performance of polymer matrix nanocomposites has not yet been studied. In this work, three types of ZrW_2O_8 were synthesized under different hydrothermal conditions, resulting in distinctly different morphologies and CTE values. The nanoparticles were then characterized and selected to reinforce epoxy resins at different loading levels. An in-depth investigation of the influence of certain properties (such as particle size, thermal expansivity, and surface area) on the rheological, thermo-mechanical, and dielectric properties of epoxy nanocomposites was conducted.

2. EXPERIMENTAL SECTION

2.1. Materials. The chemicals used for the synthesis of ZrW_2O_8 nanoparticles with different morphologies included zirconium oxynitrate hydrate ($ZrO(NO_3)_2{\cdot}xH_2O$), zirconium acetate ($Zr(C_2H_3O_2)_4$) solution in dilute acetic acid (Zr 16%), zirconium perchlorate hydrate ($ZrO(ClO_4)_2{\cdot}xH_2O$), and sodium tungstate dihydrate ($Na_2WO_4{\cdot}2H_2O$). The chemicals were all purchased from Sigma-Aldrich (St. Louis, MO). The epoxy resin used in this experiment was bisphenol A diglycidyl ether (EPON 828), purchased from Hexion Specialty Chemicals, Inc. The curing agent was a fatty polyamide formed by tall-oil fatty acids with triethylenetetramine (Versamid 140), purchased from Cognis/BASF (Germany).

2.2. Synthesis of ZrW_2O_8 Nanoparticles. During hydrothermal synthesis of ZrW_2O_8 nanoparticles with varying morphologies, the experimental conditions were controlled, as described extensively in our previous work.[33] Three types of precursor nanoparticles ($ZrW_2O_7(OH)_2{\cdot}2H_2O$) were obtained under the following hydrothermal conditions (using a 125 mL Parr pressure vessel): 0.08 M $ZrO(ClO_4)_2{\cdot}xH_2O$ and 0.10 M $Na_2WO_4{\cdot}2H_2O$ reacted in 7 M HCl at 160 °C for 12 h; 0.08 M $ZrO(NO_3)_2{\cdot}xH_2O$ and 0.10 M $Na_2WO_4{\cdot}2H_2O$ reacted in 7 M HCl at 130 °C for 12 h; 0.08 M $Zr(C_2H_3O_2)_4$ solution and 0.10 M $Na_2WO_4{\cdot}2H_2O$ reacted in 7 M HCl at 130 °C for 12 h. After the reactions were completed, white precipitates were removed from the vessel and centrifuged 5−6 times with deionized water to remove residual acids. After drying in a vacuum oven at 75 °C for 24 h, fine white powders of $ZrW_2O_7(OH)_2{\cdot}2H_2O$ were obtained by gently grinding with a mortar and pestle. The final ZrW_2O_8 powders were obtained by calcination of the precursor powders at 600 °C for 30 min.

2.3. Preparation of ZrW_2O_8/Epoxy Nanocomposites. ZrW_2O_8/epoxy nanocomposites were processed by blending the nonsurface functionalized nanoparticles directly into the epoxy resin at a mixing ratio of 70 wt % EPON 828 and 30 wt % Versamid 140[34] to investigate the thermal and physical properties of pristine nanoparticles' influence on the performance of epoxy resin. Initially, ZrW_2O_8 nanoparticles were ground gently with a mortar and pestle several times to break the fine powders apart after they were heated to 150 °C for 30 min to remove the residual hydrates observed in previous work.[33,35] Then, the ZrW_2O_8 nanoparticles were manually mixed with the epoxy resin in a silicone rubber mold (20 mm × 20 mm × 3.5 mm) and placed into a planetary mixer for high speed mixing and deaeration. Finally, after all air bubbles were removed, the mold filled with the uniform nanocomposite suspension was moved to a convection oven and cured at 120 °C for 15 h. The rectangular samples were then removed from the mold and used for further characterization.

2.4. Characterization. The morphology of the synthesized ZrW_2O_8 nanoparticles was characterized using an FEI Quanta 250 field emission scanning electron microscope (FE-SEM) at 10.00 kV under high vacuum. Ultrathin film samples with a thickness of ca. 50 nm were sliced using an ultramicrotome in order to measure the dispersion of nanoparticles in the epoxy resin utilizing a JEOL 2100 scanning and transmission electron microscope (STEM) with an accelerating voltage of 200 kV. X-ray Diffraction (XRD) patterns of synthesized ZrW_2O_8 nanoparticles and prepared epoxy nanocomposites were obtained by using Scintag powder XRD instrument with Cu Kα radiation (λ = 1.5418 Å) at 40 kV/30 mA with scan step of 0.01° scanning from 10° to 40°. The effects of loading and nanoparticle morphology on viscosity were characterized using an AR2000EX rheometer (TA Instruments). With the use of parallel plate rheology, the shear rate was increased continuously from 0 to 100 s^{-1} at room temperature. The effect of filler loading and morphology on the gel point of the epoxy resin was also studied using parallel plate oscillatory rheology measurements. The environmental control chamber was equilibrated at a temperature of 60 °C under nitrogen purge. The test mode involved two steps: initially the oscillatory strain was set at 5% until the oscillatory stress reached 1000 Pa; once this point was reached, the oscillatory stress was held at 1000 Pa.

A Q50 thermogravimetric analyzer (TGA) from TA Instruments was employed to determine the thermal stability of the epoxy resin and the residual weight of the nanoparticulate ZrW_2O_8 at different loading levels. Alumina pans were loaded with approximately 8 mg of bulk samples and heated from room temperature (25 °C) to 800 °C at a rate of 20 °C/min under air flow. Analysis of the thermal-mechanical behavior was performed on a Q400 thermo-mechanical analyzer (TMA) from TA Instruments. To prepare samples, the ZrW_2O_8-reinforced epoxy resin samples were cut into five cubic specimens (3 mm × 3 mm × 3 mm). The specimens were first heated up to 130 °C at a rate of 10 °C/min to erase the thermal history and the effect of the generated γ-phase ZrW_2O_8 during polymerization of the nanocomposites;[27] subsequently, they were cooled to 35 °C at a rate of 3 °C/min. The CTE values were determined after the second heating cycle, up to 125 °C at a rate of 3 °C/min. The dynamic-mechanical properties of the nanocomposites were determined using a Q800 dynamic mechanical analyzer (DMA) from TA Instruments. Three more specimens with dimensions of 6 mm × 3 mm × 1 mm were cut and tested in three-point bending mode. These specimens were first cooled to −20 °C and then heated to 200 °C at a rate of 3 °C/min. Data were collected between −20 to 200 °C at an amplitude of 10 μm and a frequency of 1 Hz.

The dielectric properties, including relative permittivity, loss factor, and dielectric breakdown strength, of the nanocomposites were characterized using a broadband dielectric spectrometer from Novocontrol, Inc. and a dielectric rigidity instrument from CEAST/Instron at room temperature. To determine the dielectric constant, the prepared samples (20 mm × 20 mm × 1 mm) were first sputtered with a silver coating in the shape of a 20 mm diameter circle on both surfaces of the samples. The sputtering was performed under argon purge on an Edwards Pirani coater. The samples were fixed between

two disk electrodes before the test was performed within a frequency range from 1 to 10^6 Hz. To characterize the dielectric breakdown strength, the bottom side of the samples (20 mm × 20 mm × 0.5 mm) was fully sputtered by silver while 10 small spots were sputtered on the top side using the same coating instrument. The samples were then placed between the probes of a dielectric rigidity instrument, where the upper probe was positioned directly on the sputtered spots. The breakdown voltage for each testing spot was measured as the voltage was increased by 0.5 kV/s and the current was maintained at 10 mA.

3. RESULTS AND DISCUSSION

On the basis of previous work,[33] three types of $ZrW_2O_7(OH)_2 \cdot 2H_2O$ nanoparticles with distinct morphologies were synthesized under different hydrothermal experimental conditions. Figure 1 (a–c) compares the morphologies of the three types

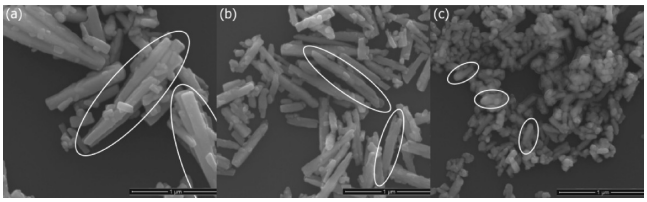

Figure 1. SEM images of three types of ZrW_2O_8 nanoparticles with different morphologies: (a) Type-1 ZrW_2O_8 nanoparticles; (b) Type-2 ZrW_2O_8 nanoparticles; (c) Type-3 ZrW_2O_8 nanoparticles.

of ZrW_2O_8 nanoparticles calcined from the precursor $ZrW_2O_7(OH)_2 \cdot 2H_2O$. Several other important properties of the nanoparticles characterized in previous work, including the crystallite size, BET surface area, and CTE value, are listed in Table 1. As highlighted in the Figure 1, it is shown that Type-1 and Type-2 ZrW_2O_8 exhibited morphologies resembling bundles consisting of 3–5 nanorods and single individual rods, respectively, with larger particle size and higher aspect ratio than those of Type-3 ZrW_2O_8. According to Table 1, in addition to lower surface area shared by Type-1 and Type-2 nanoparticles, both exhibited more negative thermal expansivities in the α-phase than Type-3 ZrW_2O_8. The mechanism behind the variation in CTE among three ZrW_2O_8 nanoparticles was also provided in our previous work.[33]

Figure 2 shows the dispersion of ZrW_2O_8 nanoparticles with different morphologies and loading levels in the cured epoxy resin. The nanoparticles were homogeneously distributed in the polymer matrix independent of loading level, which can be attributed to proper mixing procedures applied during the preparation of the specimens. It is worthwhile to note that some small fragments were observed in the matrix, especially in

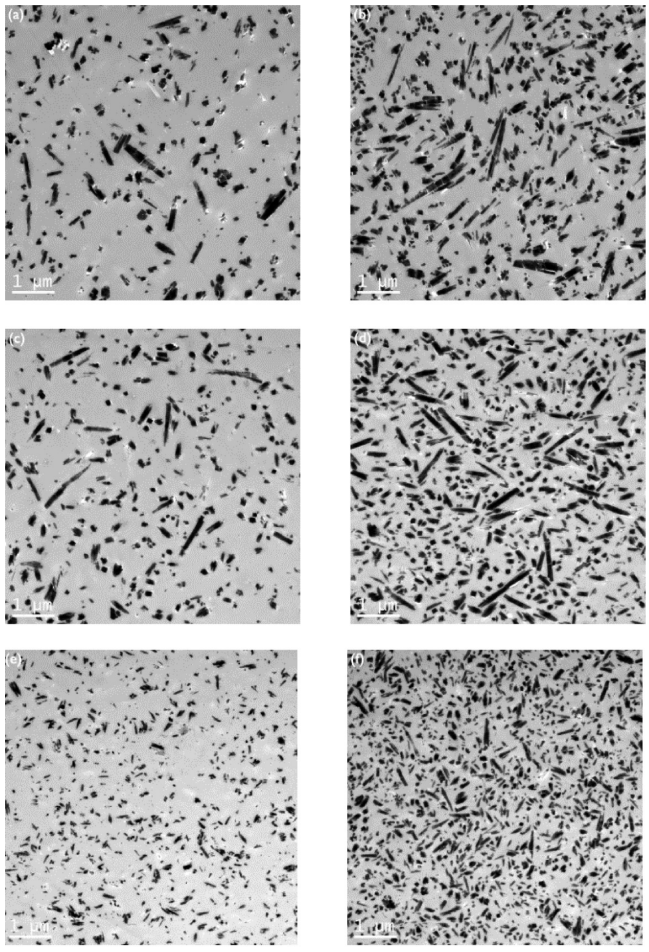

Figure 2. TEM images of ZrW_2O_8/epoxy nanocomposites with different types and volume fractions of nanoparticles: (a) 10 vol % Type-1 ZrW_2O_8; (b) 20 vol % Type-1 ZrW_2O_8; (c) 10 vol % Type-2 ZrW_2O_8; (d) 20 vol % Type-2 ZrW_2O_8; (e) 10 vol % Type-3 ZrW_2O_8; (f) 20 vol % Type-3 ZrW_2O_8.

Figure 2a,c. They can be explained by the fact that long nanorods were more vulnerable to be torn into smaller pieces under the high shear stress generated during the high-speed mixing procedure than smaller nanoparticles. The white spots and voids seen in the images are the result of filler materials that were removed from the resin during sectioning ultrathin films for TEM characterization, which may due to the weak interfacial interaction between the untreated nanoparticles and epoxy resin.

Table 1. Physical Description of Three Types of ZrW_2O_8 Nanoparticles

nanoparticle type	morphology	size scale (nm) and aspect ratio	crystallite size (nm)	surface area (m^2/g)	CTE value (ppm/°C)	
					α-phase	β-phase
1	Large, bundle-like rods	L: 900–1400 W: 80–130 L/W: ~13	50 ± 4	9.96	−11.4 ± 0.352	−4.55 ± 0.341
2	Large, rectangular rods	L: 600–1200 W: 70–120 L/W: ~10	46 ± 4	13.9	−11.2 ± 0.420	−4.65 ± 0.283
3	Small, capsule-like, short rods	L: 100–400 W: 40–60 L/W: ~6	32 ± 5	20.3	−9.25 ± 0.243	−4.94 ± 0.161

The representative powder XRD patterns of Type-1 ZrW_2O_8 nanoparticles, neat epoxy resin and Type-1 ZrW_2O_8/epoxy nanocomposites at two different volume fractions are given in Figure 3. The synthesized ZrW_2O_8 nanoparticles from

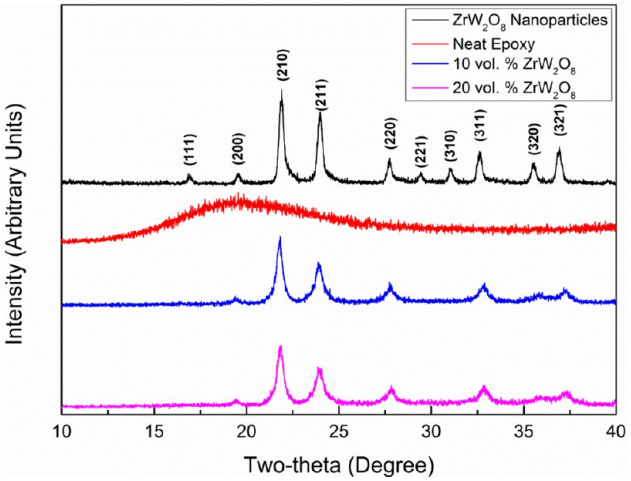

Figure 3. XRD patterns of ZrW_2O_8, neat epoxy, and ZrW_2O_8/epoxy nanocomposites.

hydrothermal reaction exhibited no measurable impurity such as tungsten oxide.[36] The ZrW_2O_8/epoxy nanocomposites displayed the feature peaks of pure α-ZrW_2O_8 compared with the amorphous characteristic of neat epoxy. Because of the incorporation of nanofillers in an amorphous matrix, the XRD patterns of nanocomposites showed the reduction in overall intensity of (*hkl*) peaks and the absence of several small peaks such as (111), (221) and (310) compared to the XRD of ZrW_2O_8 nanopowders.

Figure 4 shows a neat epoxy resin which underwent thermal degradation in a temperature range from approximately 300 to

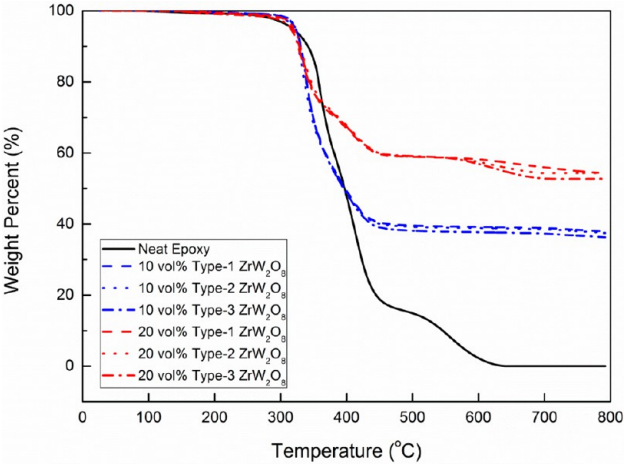

Figure 4. Comparison of TGA measurements for ZrW_2O_8/Epoxy nanocomposites.

650 °C. The weight loss of the nanocomposite after complete degradation at 800 °C was used to determine the filler loading for each specimen. The weight residues of the epoxy nanocomposites containing the three types of ZrW_2O_8 at different loadings are summarized in Table 2. It can be seen that they were in agreement with the calculated weight percent for both 10 vol % (37 wt %) and 20 vol % (54 wt %). The thermal stability of the samples was determined from the onset temperature at which 5% weight loss was observed. No obvious change in the onset temperature between neat epoxy resin and the ZrW_2O_8/epoxy nanocomposites was detected, suggesting that the addition of ZrW_2O_8 had no detrimental effect on the thermal stability of the nanocomposites.

The effects of nanoparticle properties and loading levels on the viscosity of the epoxy matrix nanocomposites were investigated under shear rates ranging from 1 to 100 s^{-1}. Figure 5 shows that the viscosity of the nanocomposites

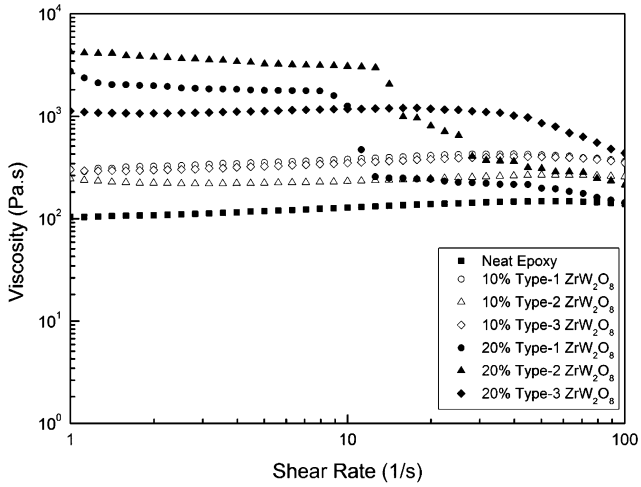

Figure 5. Comparison of viscosity of ZrW_2O_8/Epoxy suspensions.

increased with increasing filler loading, which indicated intensive interaction between higher numbers of nanoparticles with the epoxy resin. Interestingly, the rheological properties of the epoxy suspension were influenced by the morphology of incorporated nanofillers as well. For instance, the epoxy resins contained Type-1 and Type-2 ZrW_2O_8 (characterized by larger particle size and aspect ratio) showed the higher initial viscosities (approximately 3000 and 5000 Pa·s, respectively), and exhibited a noticeable shear thinning behavior, which was a result of the alignment of nanorods with high aspect ratio in epoxy under increment of shear rate.

The gelation is identified as the point at which the storage shear modulus (G') and the loss shear modulus (G'') intersects, as represented in the inset in Figure 6. A comparison of the gelation time of the neat epoxy and the nanocomposites containing different types and loadings of nanoparticles shows that the gel time diminished with increasing volume fraction of all three types of nanoparticles. As indicated in previous work,[37]

Table 2. Weight Residue and Onset Thermal-Degradation Temperature of Epoxy Resin and ZrW_2O_8/Epoxy Nanocomposites

		Type-1 ZrW_2O_8		Type-2 ZrW_2O_8		Type-3 ZrW_2O_8	
sample	neat epoxy	10 vol %	20 vol %	10 vol %	20 vol %	10 vol %	20 vol %
Weight percent (%)	0	37.90	54.30	37.50	54.34	36.3	52.74
Temperature at 5% weight loss (°C)	318.59	323.05	319.87	318.96	320.99	323.11	316.25

dx.doi.org/10.1021/am402242g | ACS Appl. Mater. Interfaces 2013, 5, 9478−9487

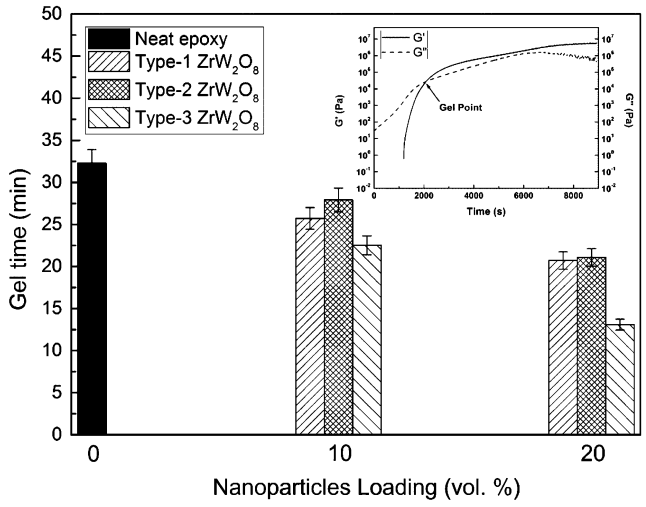

Figure 6. Representation of gel point determination and comparison of gelation time of the neat epoxy resin and the ZrW_2O_8/epoxy nanocomposites.

the reduction in gel time may be attributed to two factors: (1) a cross-linking reaction was promoted by the "catalytic effect" between the hydroxyl groups terminated on the surface of the nanoparticles and the epoxy resin; and (2) ZrW_2O_8 nanoparticles affect the rheological properties of prepolymer epoxy suspensions by increasing the elastic response of the composites. Type-3 ZrW_2O_8 characterized by higher surface area led to a higher numbers of hydroxyl groups available, which facilitated to "catalytic effect" in the network formation of epoxy, and thus further reduces the time for gelation as present in Figure 6.

Type-2 ZrW_2O_8 nanoparticles were selected to study the effect of filler loading on thermal strain in epoxy nanocomposites. Figure 7 shows that all specimens exhibited a gradual change in slope of thermal strain vs temperature curves, which represented the onset of glass transition between a glassy and a rubbery region. Furthermore, the magnitude of thermal strain gradually decreased as the filler loading increases, which was an obvious consequence of the specimens' lower thermal

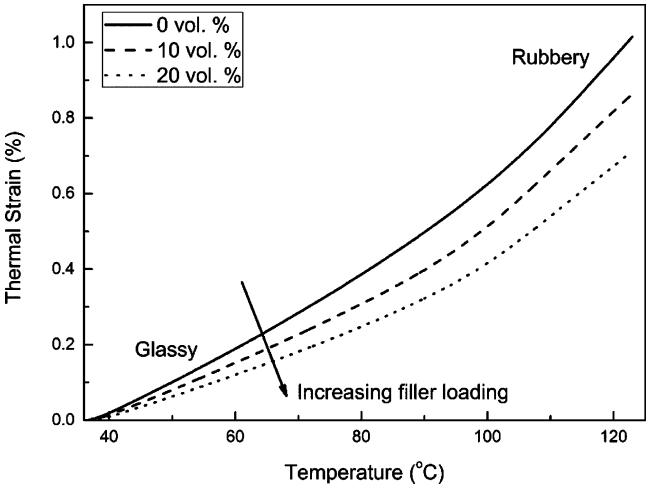

Figure 7. Comparison of the effect of filler loading levels on thermal strain in ZrW_2O_8/epoxy nanocomposites reinforced with Type-2 nanoparticles.

expansivity caused by the inclusion of the negative CTE ZrW_2O_8 nanoparticles. Consequently, ZrW_2O_8/epoxy nanocomposites improved the dimensional stability compared to neat epoxy resin.

The CTE value of the glassy region was determined by the slope of the linear regression between 50 and 70 °C, while the CTE value of the rubbery region was measured from the slope of the linear regression from 105 to 120 °C, based on eq 1.

$$\alpha = \frac{L}{L_0}\frac{\mathrm{d}L}{\mathrm{d}T} \tag{1}$$

where L_0 is the initial length of the sample and L is the length at temperature T. Figure 8a shows the CTE values of the nanocomposites reinforced by three types of ZrW_2O_8 nanoparticles at two filler-loading levels in the glassy region. The neat epoxy resin had a CTE of 87.8 ± 1.60 ppm/°C. Addition of 10 vol % ZrW_2O_8 decreased the CTEs of the nanocomposites by different amounts depending on the types of nanoparticles. Specifically, the Type-1, Type-2, and Type-3 nano-ZrW_2O_8 reduced CTE of epoxy resin by 18%, 17%, and 11% respectively. At higher loading levels (20 vol %) of nanofillers the decrease in CTE was more pronounced. Here, with Type-1 nanoparticles the CTE decreased approximately by 29%, with Type-2 nanoparticles it decreased by 27%, while a 23% CTE reduction was achieved with Type-3 nanoparticles. As expected, the CTE of the nanocomposites in the rubbery region decreased with increasing loadings for all three types of nanofillers as shown in Figure 8b. Specimens reinforced by Type-1 ZrW_2O_8 exhibits the highest CTE reduction with 29% at a loading level of 20 vol. %, followed by specimens reinforced by Type-2 and Type-3 nanoparticles that had CTE reduction for 21% and 19%, respectively.

The differences in CTE reduction for composites containing different types of ZrW_2O_8 nanoparticles can be explained by examining the thermal expansivities of the individual nanoparticles. As reported in our earlier paper,[33] wide-angle X-ray scattering experiments over a range of temperatures showed that Type-1 and Type-2 ZrW_2O_8 particles have lower CTE values (−11.2 and −11.4 ppm/°C, respectively) than Type-3 nanoparticles (−9.3 ppm/°C) in the α-phase (see Table 1). As a result, the Type-1 and Type-2 nanoparticles reduced the CTE in both the glassy and rubbery regions greater than composites reinforced with Type-3 nanoparticles at equal loading fractions.

Nanocomposites containing Type-3 ZrW_2O_8 nanoparticles were used to examine the impact of filler volume fraction on dynamic-mechanical properties. As presented in Figure 9, the reinforcement of ZrW_2O_8 nanoparticles is recognized from an increase of dynamic storage modulus (E') in both glassy and rubbery regions upon increasing filler loadings. The effects of different types and loadings of nanoparticles on the E' at 25 °C are compared in Figure 10a. Each nanoparticulate-reinforced epoxy resin showed elevated E' values due to the higher Young's modulus of ZrW_2O_8 (88.3 GPa).[38] In addition, the overall enhancement in E' of nanocomposites was nearly equal regardless the types of reinforced nano-ZrW_2O_8 at identical composition. The specimen reinforced by Type-2 nanoparticles exhibited a higher increase by 59% compared with samples containing Type-1 and Type-3 nano-ZrW_2O_8 (44% and 41%, respectively) at 10 vol %; the improvement extents were almost equivalent among the epoxy nanocomposites at 20 vol %. This indicated that the morphology of nanoparticles had no

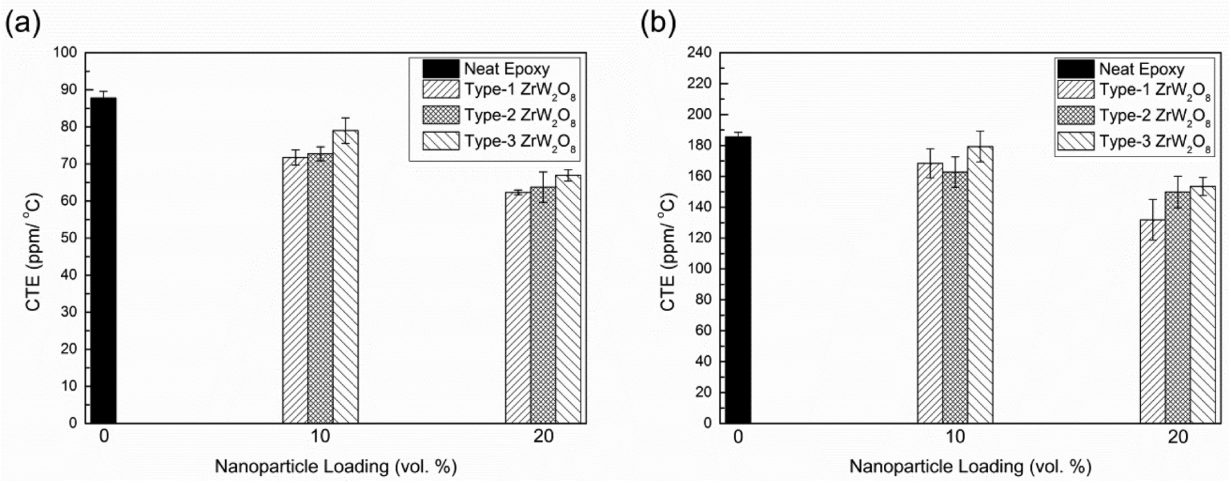

Figure 8. Comparison of the CTE values of neat epoxy resin and ZrW_2O_8/epoxy nanocomposites in the (a) glassy region and (b) rubbery region. The error bars represent standard deviations, based on five samples.

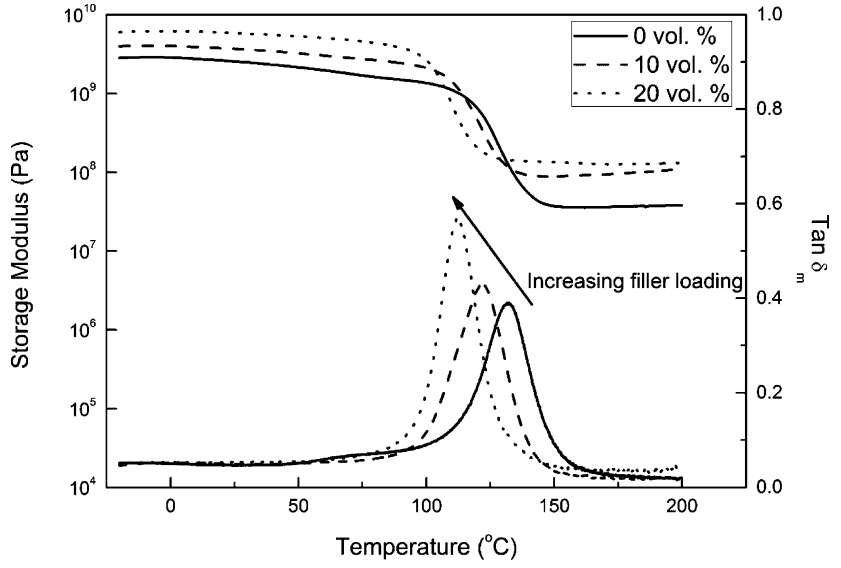

Figure 9. Comparison of dynamic-mechanical properties of ZrW_2O_8/epoxy nanocomposites.

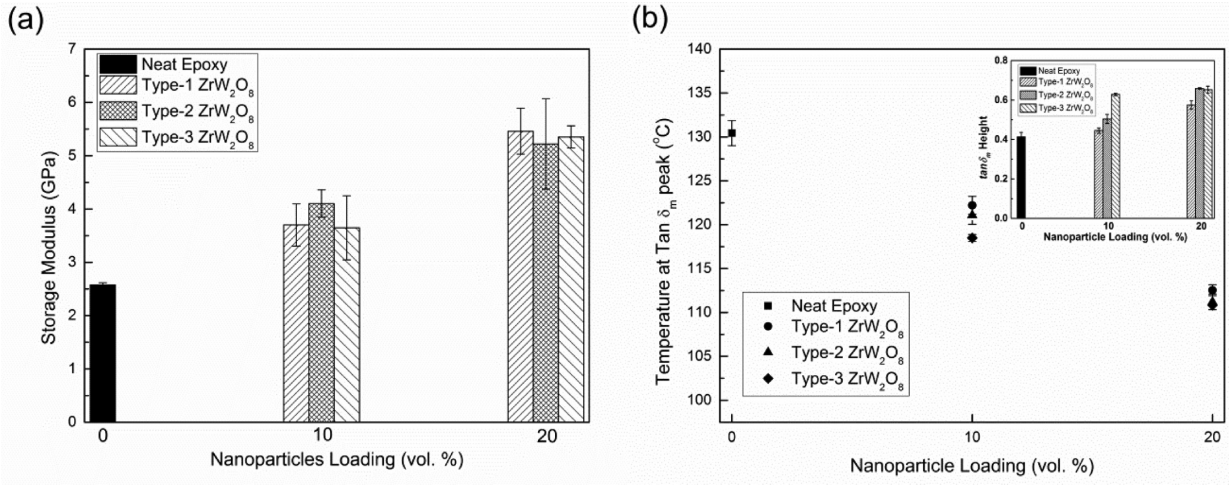

Figure 10. Comparison of (a) the storage modulus (E') at 25 °C; (b) T_g and cross-linking density measured from the tan δ_m peaks of ZrW_2O_8/epoxy nanocomposites. The error bars represent standard deviations based on three samples.

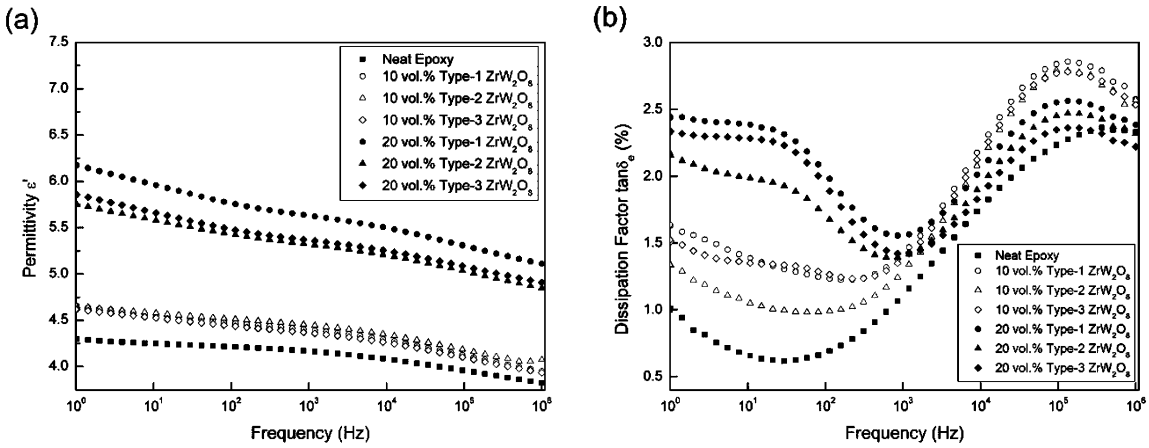

Figure 11. Comparison of (a) dielectric constant and (b) dissipation factor of ZrW_2O_8/epoxy nanocomposites.

considerable influence on the overall reinforcement effect in epoxy matrix.

Besides the variation of E', the comparison in loss factor (tan δ_m) of ZrW_2O_8/epoxy nanocomposites is illustrated in Figure 9 as well. The magnitude of tan δ_m manifests the damping effect in polymer chains network, which is determined using eq 2:

$$\tan \delta_m = \frac{E''}{E'} \tag{2}$$

where E'' is the dynamic loss modulus. Upon increasing filler loadings, the observed increase in height of tan δ_m relaxation peak can be associated with a decrease in the cross-link density of the epoxy resin,[39] and the peak position shift to lower temperature can be demonstrated the decreasing in glass transition temperatures (T_g). According to previous studies,[40,41] several factors may affect the T_g including tacticity and molecular weight of polymer. In this experiment, both neat epoxy and ZrW_2O_8/epoxy nanocomposites were processed under same condition; therefore, the introduction of plasticizer (nanoparticles) was mainly responsible for influencing T_g. Furthermore, during sample preparation, the nanopowders were dried to eliminate any moisture effects[42] and the specimens to be characterized were prepared with 1 mm thickness rather than as ultrathin polymer films.[43] Therefore, such phenomena can be explained as follow: due to the weak interfacial interaction between untreated nanoparticles and epoxy resin, the introduced nanoparticles mitigated the entanglement of the molecular chain by inhibition of the network formation and enhanced the mobility of the polymer chains in the resin system,[44,45] decreasing the cross-link density of epoxy.[46]

As seen in Figure 10b, all three types of nanoparticles facilitated a reduction in T_g as filler loading increased. Whereas the nanocomposites reinforced by Type-3 ZrW_2O_8 showed a reduction in T_g by 12.0 °C, the other samples containing Type-1 and Type-2 nanoparticles at 10 vol % loading level showed a T_g reduction of just 8.2 and 9.4 °C, respectively. Furthermore, the smaller Type-3 particles showed a higher value of tan δ_m (0.63) than that of composites from Type-1 and Type-2 particles, as shown in the inset of Figure 10b for 10 vol %. A similar relationship between T_g and the maximum value of tan δ_m was also noticed at 20 vol %. On the basis of the previous study,[47] smaller nanoparticles with higher surface areas were assumed to provide a greater disruption to the network or create more interphase with repulsive interfacial interaction, both of which were responsible for a pronounced diminishing in cross-linking density and T_g.

The effect of the morphologies and volume fractions of the ZrW_2O_8 nanoparticles on the dielectric constant (ε') and the dissipation factor (tan δ_e) of the epoxy composites was also characterized. Because the orientation of dipoles in polymer chains is dependent on frequency,[48] the ε' of neat epoxy decreased as the frequency changes from 1 to 10^6 Hz in Figure 11a. The incorporated ZrW_2O_8 nanofillers steadily increased the relative permittivity over a wide frequency range without changing the frequency dependence trend, which was the consequence of the higher permittivity of ZrW_2O_8 ($\varepsilon' \sim 10$)[49] and the accumulation of electric charge at the extended interfaces between nanoparticles and epoxy resin induced by interfacial polarization.[50,51] At lower loading, no significant difference in ε' of the nanocomposites was observed for all three types of ZrW_2O_8. Figure 11b shows tan δ_e as a function of ZrW_2O_8 type and loading. The dielectric loss tangent is defined as

$$\tan \delta_e = \frac{\varepsilon''}{\varepsilon'} \tag{3}$$

where ε'' is the dielectric loss. Because the dielectric loss of ZrW_2O_8 is dependent on the frequency at room temperature,[52] the increasing trend of tan δ_e for nanocomposites upon increasing volume fraction was more significant at low frequency ($1-10^3$ Hz) than high frequency ($10^3 \sim 10^6$ Hz). The slight increase in tan δ_e with increasing nanofiller could originate from the combination of interfacial loss induced by excessive polarized interfaces and conduction loss from the presence of charge carriers introduced by ZrW_2O_8.[48,53] However, the morphology of nanoparticle did not substantially influence the dielectric properties of the nanocomposites.

The dielectric breakdown strength represents the capability of an insulator to withstand electrical stress before electrical failure occurs. It is measured using electrical breakdown voltage with respect to sample thickness. Figure 12 shows that the breakdown strength was not deteriorated for any ZrW_2O_8/epoxy nanocomposite compared to neat epoxy resin (23.46 ± 3.198 MV/m). However, the error bars determined from the standard deviation based on ten measured points were not identical among the tested samples. To identify the distribution of electrically weak points that are randomly present on

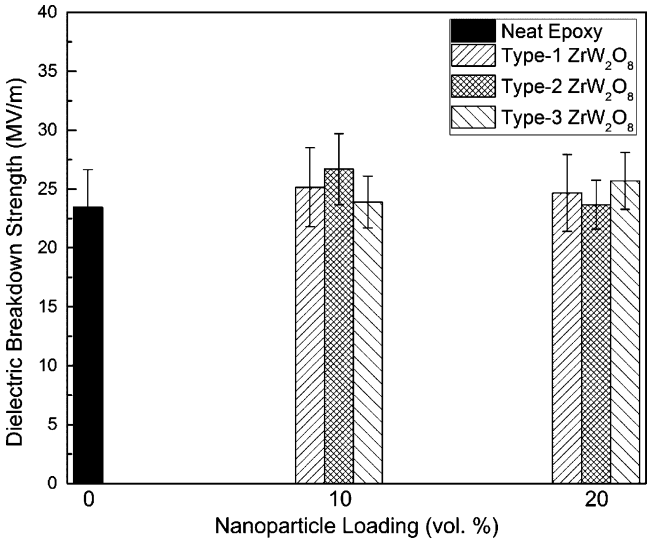

Figure 12. Comparison of the dielectric breakdown voltage of ZrW_2O_8/Epoxy nanocomposites. The error bars represent standard deviations based on ten measurements.

identical samples, applying a statistical analysis of the measured breakdown strength data of the ZrW_2O_8/epoxy nanocomposites is necessary.

The cumulative distribution function (CDF) of the dielectric breakdown strength with Weibull method was applied to investigate the distribution of dielectric breakdown behavior of identical specimens as studied in previous work.[54] The CDF for a two-parameter Weibull distribution is determined using eq 4:

$$F(E;\alpha,\beta) = 1 - \exp\left[-\left(\frac{E}{\alpha}\right)^{\beta}\right] \tag{4}$$

where F is the probability of the sample exhibiting electrical failure, E is the measured dielectric breakdown strength, and α and β represent the scale and shape of the sample and are obtained by least-squares regression. With Y_i and X_i given by eqs 5 and 6, respectively:

$$X_i = \ln\{-\ln[1 - F(i, N)]\} \tag{5}$$

$$Y_i = \ln(E_i) = mX_i + c \tag{6}$$

CDF of the probability of breakdown $F(i, N)$ is estimated by eq 7

$$F(i, N) = \frac{i - 0.3}{N + 0.4} \tag{7}$$

where, N is the total number of tested dielectric breakdown voltages and i is the assigned order for dielectric strengths, ranking from smallest to largest. The slope (m) and intercept (c) are defined as

$$m = \frac{\sum_i^N (X_i - \bar{X})(Y_i - \bar{Y})}{\sum_i^N (X_i - \bar{X})^2}, \quad c = \bar{Y} - m\bar{X} \tag{8}$$

With the use of eq 9

$$\alpha = \exp(c), \quad \beta = \frac{1}{m} \tag{9}$$

both the slope and intercept can be obtained.

From the Weibull analysis of the breakdown strength shown in Figure 13a, the data collected from 10 dielectric breakdown strength points for each testing specimen varied between 19 and 32 MV/m. The linear slopes of the CDFs, which is a measure of the variability of breakdown strengths, are given in Figure 13a and compared in Figure 13b. In comparison with neat epoxy, Type-1 particulate-reinforced nanocomposites showed lower variability than the other systems including neat epoxy, which was also in good agreement with higher permittivity at 20 vol % loading (Figure 11a) by existence of less substantial microvoids. On the other hand, the slopes of CDFs were lower and similar to the value of neat epoxy regarding the specimen containing 20 vol % Type-2 ZrW_2O_8 and 10 vol % Type-3 nanoparticles, suggesting the greater disparity among the measured breakdown strengths. Such observation was also attributed to the presence of microdefects and agglomerated nanoparticles in the prepared samples, which was reflected by the large standard deviation of storage modulus in these specimens as well (Figure 10a).

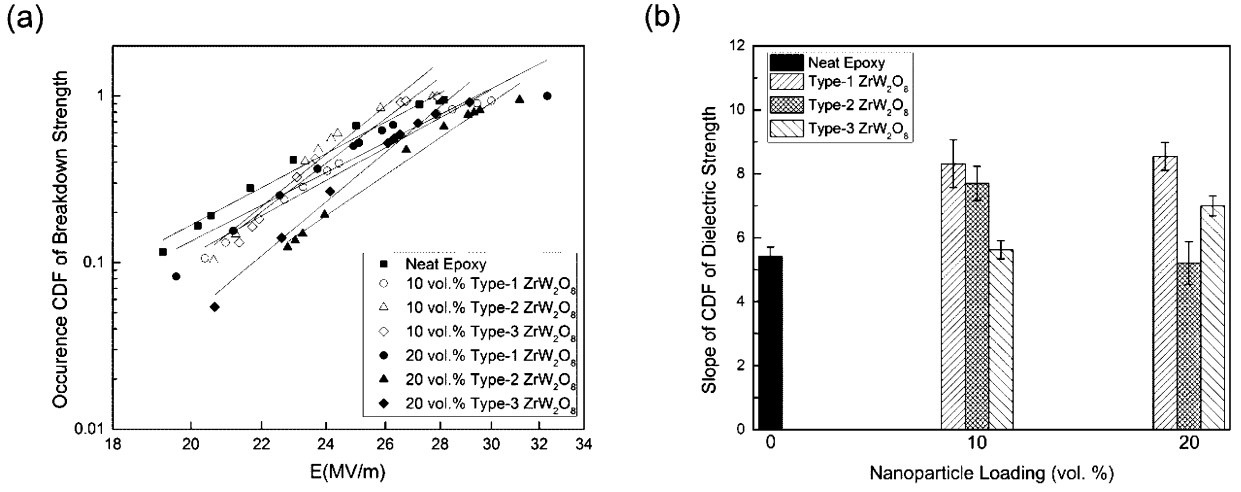

Figure 13. Comparisons of (a) the CDF of the measured dielectric strength with linear fitting slopes and (b) slope value obtained from the linear fitting of ZrW_2O_8/Epoxy nanocomposites.

dx.doi.org/10.1021/am402242g | ACS Appl. Mater. Interfaces 2013, 5, 9478−9487

4. CONCLUSION

In this work, epoxy-based nanocomposites reinforced by three types of ZrW_2O_8 nanoparticles with distinct physical and thermal properties and loading levels of 10 and 20 vol % were successfully prepared. The homogeneous dispersion of ZrW_2O_8 nanoparticles in the polymer matrix did not negatively affect the thermal stability of the composite. The viscosity of the suspension exhibited a more significant increase when reinforced by the larger nanoparticles than with the smaller ones. The gel time of the nanocomposites decreased as ZrW_2O_8 loading increased, indicating a catalytic effect of the nanoparticles on the formation of a cross-linking network. Importantly, the greatest reduction in CTEs in the glassy region was found in the specimens with 20 vol % of those ZrW_2O_8 nanoparticles that exhibited the most negative CTE values. At 25 °C, all three types of nanoparticles facilitated an overall equivalent enhancement in storage modulus of the epoxy with increasing filler loadings. However, the lowering of cross-linking density and T_g were attributed to the disruption of fully dense network and formation of repulsive interphase by presence of nanoparticles in polymer matrix. With slightly increasing nanofiller composition, both dielectric constant and dissipation factor of the nanocomposites increased slightly over the frequency range between 1 and 10^6 Hz due to the introduction of interfacial polarization effect between nanoparticles and epoxy matrix under AC electric field. Finally, the ZrW_2O_8 nanoparticles improved dielectric breakdown strength slightly, and lowered the variation of breakdown strength according to the Weibull statistical distribution analysis. In summary, epoxy reinforced with 20 vol % Type-1 ZrW_2O_8/epoxy nanocomposites achieved excellent CTE reduction, a pronounced improvement in dynamic mechanical properties, and preserved the advantageous dielectric properties of epoxy resins, making them prospective candidates for applications in the microelectronic insulation industry.

AUTHOR INFORMATION

Corresponding Author

*E-mail: MichaelR.Kessler@wsu.edu.

Notes

The authors declare no competing financial interest.

ACKNOWLEDGMENTS

The authors gratefully acknowledge partial funding for this project from Honeywell Federal Manufacturing & Technologies, LLC and the Air Force Office of Scientific Research (Award No. FA9550-12-1-0108). The authors also acknowledge Tracey Pepper (Genetics, Development & Cell Biology, Iowa State University) for her assistance with TEM measurements.

REFERENCES

(1) Messersmith, P. B.; Giannelis, E. P. *Chem. Mater.* **1994**, *6*, 1719.
(2) Gojny, F. H.; Wichmann, M. H. G.; Fiedler, B.; Kinloch, I. A.; Bauhofer, W.; Windle, A. H.; Schulte, K. *Polymer* **2006**, *47*, 2036.
(3) Montazeri, A.; Javadpour, J.; Khavandi, A.; Tcharkhtchi, A.; Mohajeri, A. *Mater. Des.* **2010**, *31*, 4202.
(4) Li, Y. Q.; Fu, S. Y.; Mai, Y. W. *Polymer* **2006**, *47*, 2127.
(5) Chen, C. G.; Justice, R. S.; Schaefer, D. W.; Baur, J. W. *Polymer* **2008**, *49*, 3805.
(6) Kang, S.; Hong, S. I.; Choe, C. R.; Park, M.; Rim, S.; Kim, J. *Polymer* **2001**, *42*, 879.
(7) Olmos, D.; Martinez, F.; Gonzalez-Gaitano, G.; Gonzalez-Benito, J. *Eur. Polym. J.* **2011**, *47*, 1495.
(8) Goertzen, W. K.; Kessler, M. R. *J. Therm. Anal. Calorim.* **2008**, *93*, 87.
(9) Jang, J. S.; Varischetti, J.; Lee, G. W.; Suhr, J. *Composites, Part A* **2011**, *42*, 98.
(10) Zhi, C. Y.; Bando, Y.; Tang, C. C.; Kuwahara, H.; Golberg, D. *Adv. Mater.* **2009**, *21*, 2889.
(11) Abdalla, M.; Dean, D.; Theodore, M.; Fielding, J.; Nyairo, E.; Price, G. *Polymer* **2010**, *51*, 1614.
(12) Kim, S. K.; Kim, J. T.; Kim, H. C.; Rhee, K. Y.; Kathi, J. *J. Macromol. Sci., Part B: Phys.* **2012**, *51*, 358.
(13) Yasmin, A.; Luo, J. J.; AbCot, J. L.; Daniel, I. M. *Compos. Sci. Technol.* **2006**, *66*, 2415.
(14) Mary, T. A.; Evans, J. S. O.; Vogt, T.; Sleight, A. W. *Science* **1996**, *272*, 90.
(15) Evans, J. S. O.; David, W. I. F.; Sleight, A. W. *Acta Crystallogr., Sect. B: Struct. Sci.* **1999**, *55*, 333.
(16) Sun, L.; Sneller, A.; Kwon, P. *Compos. Sci. Technol.* **2008**, *68*, 3425.
(17) Yan, X.; Cheng, X.; Xu, G.; Wang, C.; Sun, S.; Riedel, R. *Materialwiss. Werkstofftech.* **2008**, *39*, 649.
(18) Holzer, H.; Dunand, D. C. *J. Mater. Res.* **1999**, *14*, 780.
(19) Yang, X. B.; Xu, J.; Li, H. J.; Cheng, X. N.; Yan, X. H. *J. Am. Ceram. Soc.* **2007**, *90*, 1953.
(20) Chu, X. X.; Huang, R. J.; Yang, H. H.; Wu, Z. X.; Lu, J. F.; Zhou, Y. A.; Li, L. F. *Mater. Sci. Eng., A* **2011**, *528*, 3367.
(21) Miller, W.; Smith, C. W.; Dooling, P.; Burgess, A. N.; Evans, K. E. *Phys. Status Solidi B* **2008**, *245*, 552.
(22) Badrinarayanan, P.; Rogalski, M.; Wu, H.; Wang, X.; Yu, W.; Kessler, M. R. *Macromol. Mater. Eng.* **2013**, *298*, 136.
(23) Sullivan, L. M.; Lukehart, C. M. *Chem. Mater.* **2005**, *17*, 2136.
(24) Yang, J. A.; Yang, Y. S.; Liu, Q. Q.; Xu, G. F.; Cheng, X. N. *J. Mater. Sci. Technol.* **2010**, *26*, 665.
(25) Chen, M. Y.; Chen, C. G. *Polym. Adv. Technol.* **2012**, *23*, 958.
(26) Tani, J.; Kimura, H.; Hirota, K.; Kido, H. *J. Appl. Polym. Sci.* **2007**, *106*, 3343.
(27) Badrinarayanan, P.; Mac Murray, B.; Kessler, M. R. *J. Mater. Res.* **2009**, *24*, 2235.
(28) Badrinarayanan, P.; Kessler, M. R. *Compos. Sci. Technol.* **2011**, *71*, 1385.
(29) Badrinarayanan, P.; Rogalski, M. K.; Kessler, M. R. *ACS Appl. Mater. Interfaces* **2012**, *4*, 510.
(30) Shi, J. D.; J. P., Z.; Wu, K. H.; Larkins, G. *Mater. Res. Soc. Symp. Proc.* **1996**, 445.
(31) Haman, K.; Badrinarayanan, P.; Kessler, M. R. *ACS Appl. Mater. Interfaces* **2009**, *1*, 1190.
(32) Lind, C.; Coleman, M. R.; Kozy, L. C.; Sharma, G. R. *Phys. Status Solidi B* **2011**, *248*, 123.
(33) Wu, H.; Badrinarayanan, P.; Kessler, M. R. *J. Am. Ceram. Soc.* **2012**, *95*, 3643.
(34) Westerdahl, C. A. L.; Hall, J. R.; Schramm, E. C.; Levi, D. W. *J. Colloid Interface Sci.* **1974**, *47*, 610.
(35) Banek, N. A.; Baiz, H. I.; Latigo, A.; Lind, C. *J. Am. Chem. Soc.* **2010**, *132*, 8278.
(36) Badrinarayanan, P.; Ahmad, M. I.; Akinc, M.; Kessler, M. R. *Mater. Chem. Phys.* **2011**, *131*, 12.
(37) Goertzen, W. K.; Sheng, X.; Akinc, M.; Kessler, M. R. *Polym. Eng. Sci.* **2008**, *48*, 875.
(38) Drymiotis, F. R.; Ledbetter, H.; Betts, J. B.; Kimura, T.; Lashley, J. C.; Migliori, A.; Ramirez, A.; Kowach, G.; Van Duijn, J. *Phys. Rev. Lett.* **2004**, 93.
(39) Hussain, M.; Varley, R. J.; Mathys, Z.; Cheng, Y. B.; Simon, G. P. *J. Appl. Polym. Sci.* **2004**, *91*, 1233.
(40) Ash, B. J.; Siegel, R. W.; Schadler, L. S. *J. Polym. Sci., Part B: Polym. Phys.* **2004**, *42*, 4371.
(41) Sun, Y.; Zhang, Z.; Moon, K.-S.; Wong, C. P. *J. Polym. Sci., Part B: Polym. Phys.* **2004**, *42*, 3849.

(42) Sun, Y. Y.; Zhang, Z. Q.; Moon, K. S.; Wong, C. P. *J. Polym. Sci., Part B: Polym. Phys.* **2004**, *42*, 3849.
(43) Ruiz-Perez, L.; Royston, G. J.; Fairclough, J. P. A.; Ryan, A. J. *Polymer* 2008, *49*, 4475.
(44) Liu, G.; Zhang, H.; Zhang, D. J.; Zhang, Z.; An, X. F.; Yi, X. S. *J. Mater. Sci.* **2012**, *47*, 6891.
(45) Hill, D. J. T.; Perera, M. C. S.; Pomery, P. J.; Toh, H. K. *Polymer* **2000**, *41*, 9131.
(46) Preghenella, M.; Pegoretti, A.; Migliaresi, C. *Polymer* **2005**, *46*, 12065.
(47) Singha, S.; Thomas, M. J. *IEEE Trans. Dielectr. Electr. Insul.* **2008**, *15*, 12.
(48) Peng, W.; Huang, X.; Yu, J.; Jiang, P.; Liu, W. *Composites, Part A* **2010**, *41*, 1201.
(49) Sleight, A. W. *Annu. Rev. Mater. Sci.* **1998**, *28*, 29.
(50) Lu, J. X.; Moon, K. S.; Xu, J. W.; Wong, C. P. *J. Mater. Chem.* **2006**, *16*, 1543.
(51) Huang, X.; Jiang, P.; Kim, C.; Ke, Q.; Wang, G. *Compos. Sci. Technol.* **2008**, *68*, 2134.
(52) Evans, J. S. O.; Mary, T. A.; Vogt, T.; Subramanian, M. A.; Sleight, A. W. *Chem. Mater.* **1996**, *8*, 2809.
(53) Lu, J.; Moon, K. S.; Wong, C. P. *J. Mater. Chem.* **2008**, *18*, 4821.
(54) Li, L.; Bowler, N.; Hondred, P. R.; Kessler, M. R. *IEEE Trans. Dielectr. Electr. Insul.* **2011**, *18*, 1955.